NASA Technical Memorandum 89494

Results of the Integration of a Transonic Full-Potential Analysis Program with a Free-Wake Lifting-Line Program for Hovering Rotors

Song-Young Chung, Ames Research Center, Moffett Field, California

May 1987

National Aeronautics and Space Administration

Ames Research Center
Moffett Field, California 94035

NASA Technical Memorandum 89494

Results of the Integration of a Transonic Full-Potential Analysis Program with a Free-Wake Lifting-Line Program for Hovering Rotors

Song-Young Chung

May 1987

National Aeronautics and
Space Administration

SUMMARY

This report discusses the hovering performance predictions of the TFAR1 and OPLIN codes and the experimental data discussed in reference 6. The TFAR1 program solves the full-potential equation in a rotor-fixed coordinate system by use of the line relaxation method. The OPLIN program calculates the positions of wake vortices and rotor performance using the influence-coefficient-and-lifting-line method. The two programs are combined by adding the induced velocities from the OPLIN code to the near flow-field of the rotor from the TFAR1 code. Results of this investigation show that the TFAR1 program converges better with the downwash-coupling method than the twist correction method to include the wake downwash.

INTRODUCTION

Recently, several finite-difference methods using small-disturbance (refs. 1,2), full-potential (refs. 3,4), or Euler equations (ref. 5) have been used for the analysis of helicopter rotor flow. Wake effects are computed by either momentum theory or lifting surface methods. Experimental and analytical results for hovering rotors are discussed in reference 6 where the tip vortices were found to reach their maximum strength very quickly, but not in the core size or radial and axial positions. The best agreement between experiment and analytical results was obtained when the tip vortex contraction was reduced by 0.025 R (radius) from the experimental data.

After the effective angle of attack has been determined from momentum theory and blade flapping motion, the pressure distribution on a helicopter rotor was calculated in reference 1 from the small-disturbance potential equation. In reference 2, the effects of transonic flow on the advancing blade are calculated by using an unsteady, transonic small-perturbation method with a Drees downwash model. In reference 3, the full-potential equation is derived using body-conforming coordinates fixed on the rotor, and the pressure distributions computed on the advancing blade are presented for nonlifting helicopter rotors with sweep and taper. The TFAR1 program used in the present report was developed in reference 3 where the one-dimensional (1-D) and 2-D wake models were introduced. Lifting calculation for the advancing blade were presented in reference 4 where the effective angle of attack was calculated from the wake portion of the program CAMRAD (ref. 7) at each spanwise station.

In reference 5 a semi-implicit approximate factorization is used to factorize the unsteady Euler equation where the spanwise derivative is lagged behind the other

two derivatives by one time-step. This semi-implicit Euler equation is solved for wing and hovering rotors. Various finite-difference and lifting-surface methods, using acceleration or velocity potential, are reviewed with wake modelling in reference 8 for rotary wing analysis. The capability of the Euler code to capture wake vortices is discussed.

In this paper, the free-wake lifting-line program OPLIN, as developed in reference 9 and 10-14, is coupled with the program, TFAR1, for the analysis of hovering rotors with transonic tip speeds.

The author wishes to express thanks to Dr. I-Chung Chang for allowing me to couple his code, TFAR1, with my code, OPLIN.

FULL-POTENTIAL FORMULATION

The velocity components in a rotating coordinate reference frame are decomposed into the freestream component, perturbation potential, and the additional downwash caused by the wake vortices which were not captured by the transonic full-potential equation. The velocity components are

$$q_1 = v_1 + \phi_x + w_1 \tag{1}$$

$$q_2 = v_2 + \phi_y + w_2 \tag{2}$$

$$q_3 = v_3 + \phi_z + w_3 \tag{3}$$

$$v_1 = \Omega z \tag{4}$$

$$v_2 = 0 \tag{5}$$

$$v_3 = -\Omega x \tag{6}$$

where q is the total velocity, v is the velocity caused by the rotor rotation, ϕ is the perturbation potential, w is the downwash calculated everywhere by the free-wake lifting-line code in the computational domain, and Ω is the rotor rotational velocity.

The circulation Γ at each span station is defined by the potential jump at the trailing edge.

$$\Gamma = \vec{q} \cdot \vec{dr} = \nabla\Phi \cdot \vec{dr} = d\Phi = \Phi_u - \Phi_l \tag{7}$$

The potential jump is the wake vortex strength in the 3-D flow. The conservation of circulation for inviscid flow and the force-free condition on the wake are satisfied when the potential jump is convected with the local velocity. The Kutta condition defines the potential jump at the trailing edge to be the magnitude of the

circulation of the lifting body. This jump is interpolated into the numerical grid line as follows.

$$\Phi_{1u} = \Phi_{3u} + [\Phi] = \Phi_{3l} + \Delta\Phi \tag{8}$$

$$\Phi_{1l} = \Phi_{3u} - [\Phi] = \Phi_{3u} - \Delta\Phi \tag{9}$$

Here Δ represents the jump in the quantity. Also, the flow-tangency condition on the body is applied according to the following numerical boundary conditions.

$$\vec{q} \cdot \vec{n} = \frac{\partial \phi}{\Phi n} + (V + w)_n = 0 \tag{10}$$

$$\phi_3 - \phi_1 + 2\Delta n(V + w)_n = 0 \tag{11}$$

$$\phi_1 = \phi_3 + 2\Delta n(V + w)_n = 0 \tag{12}$$

FREE WAKE FORMULATION

The free-wake lifting-line theory developed in reference 8 divides the wake of a hovering rotor into a near wake attached to the blade trailing edge, an intermediate wake of several inner and tip ring vortices, and the far wake of semi-infinite vortex cylinders (fig. 1). The downwash induced by the entire wake on the rotor blade and in the wake vortices is computed as influence coefficients which are a function of wake geometry.

On the position i of the quarter-chord line of the blade, or in the intermediate wake, the induced velocities are $(w\,\vec{k} + v\,\vec{i})$, such that

$$w_i^{\nu+1} = A_{zi,j}^{\nu} \quad \gamma_i^{\nu+1}, \qquad v_i^{\nu+1} = A_{yi,j}^{\nu} \quad \gamma_j^{\nu+1} \tag{13}$$

where γ is the strength of the bound circulation, and $A_{yi,j}^{\nu}$ and $A_{zi,j}^{\nu}$ are the y- and z- direction influence coefficients at position i caused by all of the trailing vortices of bound circulation j of unit strength. The influence coefficients are computed by using the Biot-Savart law from the wake geometry of the ν th iteration. The bound circulation of the $(\nu + 1)$th iteration is computed by applying the Kutta-Joukowski law at each blade section. The wake geometry of the $(i + 1)$th position is computed by integrating the downwash on the wake positions at i and $i - 1$ as follows.

$$z_i = z_{i-1} + 0.5*(w_{i-1} + w_i)* 2\pi/b \tag{14}$$

$$r_i = r_{i-1} + 0.5*(v_{i-1} + v_i)* 2\pi/b \tag{15}$$

where z and r are the axial and radial positions of the intermediate and far-wake vortices, w and v are the corresponding induced velocities, and b is the number of blades. The r and z for $i = 0$ are the radial and axial positions of the near

wake considered to be rolled up instantaneously on the plane of rotation according to the law of conservation of linear momentum as follows.

$$(r_k - r_1)r_0^2 = \sum_{j=1}^{k} r_j^2 \Delta r_j \qquad (16)$$

The bound circulation is calculated by iteration until the wake geometry converges. The influence coefficients include, 1) the near wake, 2) the intermediate wake, and the 3) the far wake. The influence coefficients caused by the near wake which are not contained in the code, TFAR1, are computed everywhere in the near field of the blade. These influence coefficients are added to those associated with the intermediate and far wakes. By multiplying the final strength of bound circulation to the added influence coefficients, the induced velocities are computed everywhere in the near field of the rotor blade. The linear compressibility correction is made by including the lift-curve slope change in the circulation-downwash relation. The bound circulation and blade lift for a given blade geometry are calculated by iteration until the wake geometry, and hence the bound circulation, no longer changes during iteration. The wake geometry is initially generated by applying the momentum theorem, assuming constancy in the flow field, and by integrating the downwash velocities from it. The downwash caused by the wake vortices which are not contained in the computational domain of the TFAR1 code is obtained on the blade, that is, in the near field, from the calculated bound circulation and wake geometry.

RESULTS AND DISCUSSIONS

The correct position of the wake is very important to obtain correct pressure distributions. Existing finite-difference codes usually capture the near wake which is presented by the jump in potential across a flat continuation surface traced by the blade. The roll-up and nonlinear interaction of wake vortices are not included in TFAR1. The roll-up and wake geometry are computed in the free-wake lifting-line code, OPLIN, and the velocity field near the blade caused these wake vortices is computed and added to the velocity field of the finite-difference code as shown in flow chart (fig. 2). The rotor blade geometry used in the computation is shown in figure 3.

Figure 4 shows the pressure distributions from two difference calculations and experimental results at spanwise positions $r/R = 0.68, 0.80, 0.89, 0.96$, tip Mach = 0.877 and pitch = 8°. The present results of the coupling of the two programs overestimates the pressure, compared to experiments of reference 6 while the finite-difference modeling of reference 1 underestimates the pressure. The theoretical drag coefficient, Cd, is the induced drag due to downwash. All three sets of results show the shock formation near the tip, but the calculations capture the shocks behind the experimental which may be partially due to disregarding the boundary layer and partially due to the incorrect downwash field. Figure 5 shows the

wake tip-vortex positions from the experiment and the result calculated from the OPLIN code. The calculated tip-vortex value is slightly less than the experimental value. Figure 6 shows the pressure distributions obtained by the present calculation using the coupling of TFAR1 and OPLIN and the experiments of reference 6 at five different spanwise locations and at the same rotor blade condition as for figure 4. In the inboard portion of the blade, the theory overpredicts the pressure distributions and near the blade tip, the predicted shocks are behind the experimental locations.

Figure 7 compares the computed pressure distributions with the measured test data at tip Mach = 0.794. Figure 8 compares the pressure distributions at tip Mach = 0.612. In both cases, the blade is at a constant pitch of 8°. Both comparisons of calculations and experiments show the same trend shown in figure 6, that the different tip Mach number has little effect on the comparison results. Figure 9 shows the pressure distributions at tip Mach = 0.226 and pitch angle of 12°. Except at r/R = 0.5, the agreement is very good, including the suction peak-pressure distributions. Figures 10 and 11 show the pressure distributions at tip Mach = 0.610, 0.794 for a pitch angle of 12°. The computed shock positions are slightly downstream from the experiments, which may be due to the boundary layer effect. All comparisions with the experimental results show that the placing of one vortex beneath the blade tip is necessary to obtain good agreement with experiments. Figures 12 and 13 show better agreement with experiments with one vortex line correction at tip Mach = 0.794, 0.226 and pitch angle of 12°.

CONCLUSIONS

The transonic full-potential flow analysis code, TFAR1, has been modified so that the downwash from the code, OPLIN, is added to TFAR1 for hovering performance prediction. Also, TFAR1 has been upgraded to compute the flow in the propeller and wind turbine cases when the downwash caused by wakes is calculated if the mean velocity is normal to the rotordisk.

The computational efficiency remains about the same as before, but the large amount of blade twist required to include the downwash effects is replaced by the additional downwash velocity. The comparison shows that the pressure distribution is slightly better-predicted for the higher-loading case of pitch = 12° (figs. 9 and 10) than for the case of pitch = 8° (figs. 6, 7, and 8); possibly because of the smooth wake geometry and downwash field.

REFERENCES

1. Caradonna, F. X.; Tung, C.; and Desopper, A.: Finite Difference Modeling of Rotor Flows Including Wake Effects. J. Am. Helicopter Soc., Apr. 1984.

2. Desopper, A.: Study of Unsteady Transonic Flow on Rotor Blades with Different Tip Shapes, Vertica, vol. 9, no. 3, pp. 257-272, 1985.

3. Chang, I-C, Transonic Flow Analysis for Rotors: Part 1--Three dimensional, Quasi-Steady, Full-Potential Calculation", NASA TP-2375, Oct. 1984.

4. Chang, I-Chung; and Tung, Chee: Numerical Solution of the Full Potential Equations for Rotors and Oblique Wings Using a New Wake Model, AIAA Paper 85-0268.

5. Sankar, N. L.; Wake, B. E.; and Lekoudis, S. G.: Solution of Unsteady Euler Equations for fixed and Rotor Wing Configurations, J. Aircraft, vol. 23, no. 4, Apr. 1986.

6. Caradonna, F. X.; and Tung, C.: Experimental and Analytical Studies of a Model Helicopter Rotor in Hover, Vertica, vol. 5, pp. 149-161, 1981.

7. Johnson, W.: Development of a Comprehensive Analysis of Rotorcraft 1: Rotor Model and Wake Analysis, Vertica, vol. 5, no. 2, 1981.

8. Davis, Sanford S.; and Chang, 1-Chung: The Critical Role of Computational Fluid Dynamics in Rotary Wing Aerodynamics, AIAA Paper 86-0336.

9. Chung, S. Y.: Formal Optimization of Hovering Performance Using Free Wake Lifting Surface Theory, NASA CR-177103, Feb. 1986.

10. Miller, R. H.: Simplified Free Wake Analysis for Rotors, FFA (Sweden) TN-1982-7.

11. Miller, R. H.: Free Wake Techniques for Rotor Aerodynamic Analysis, Volume I: Summary of Results and Background Theory, NASa CR-166434, 1983.

12. Miller, R. H.: Factors Influencing Rotor Aerodynamics in Hover and Forward Flight, 10th European Rotorcraft Forum, Paper no. 11, 1984.

13. Miller, R. H.: A Simplified Approach to the Free Wake Analysis of a Hovering Rotor, Vertica, vol. 6, pp. 89-95, 1982.

14. Miller, R. H., Application of Fast Free Wake Analysis Techniques to Rotors, Vertica, vol. 8, no. 3, pp. 255-261, 1984.

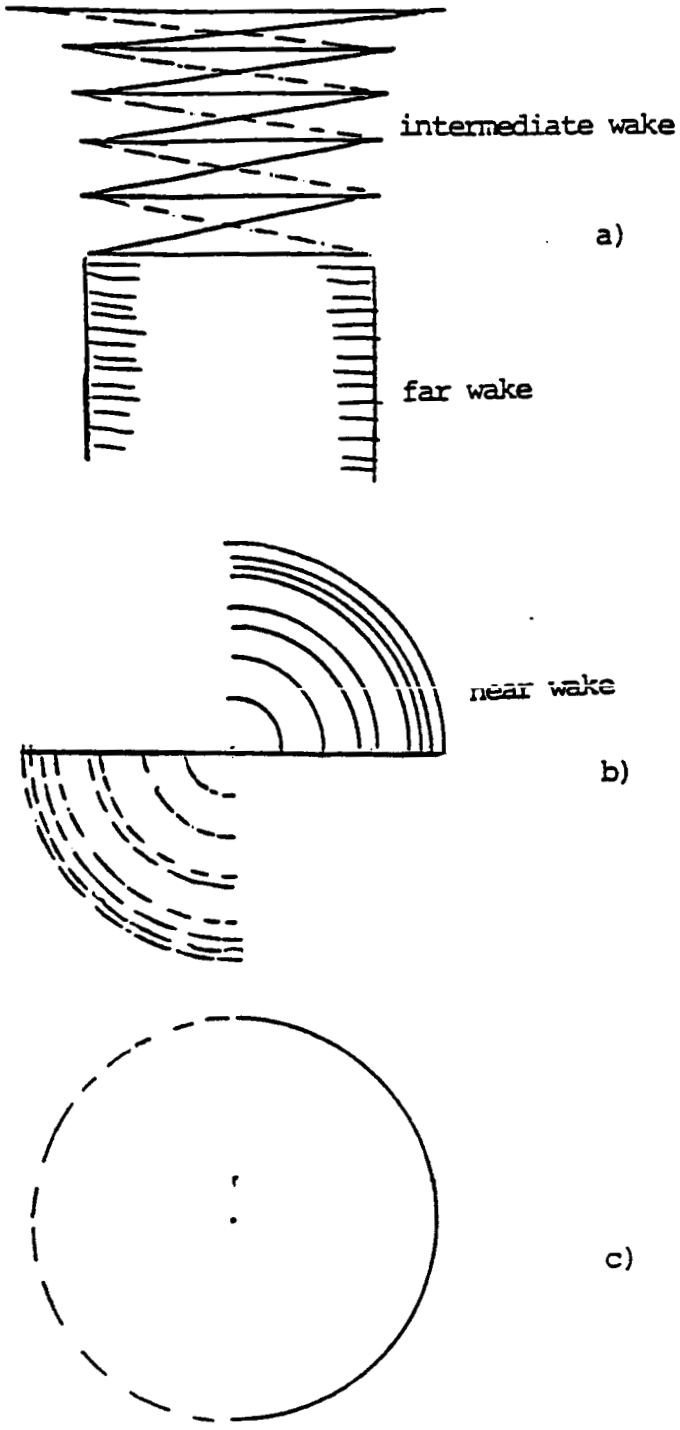

Figure 1.- Geometry of near, intermediate, and far wakes for hovering rotors using vortex rings and cylinders to represent the wake. (a) Side view of rotor wake model showing intermediate and far wakes formed from vortex spiral for 2 blades, tip vortex only shown. _____ Blade one _____ Blade two, (b) Plane view showing near wake, (c) Formation of intermediate wake.

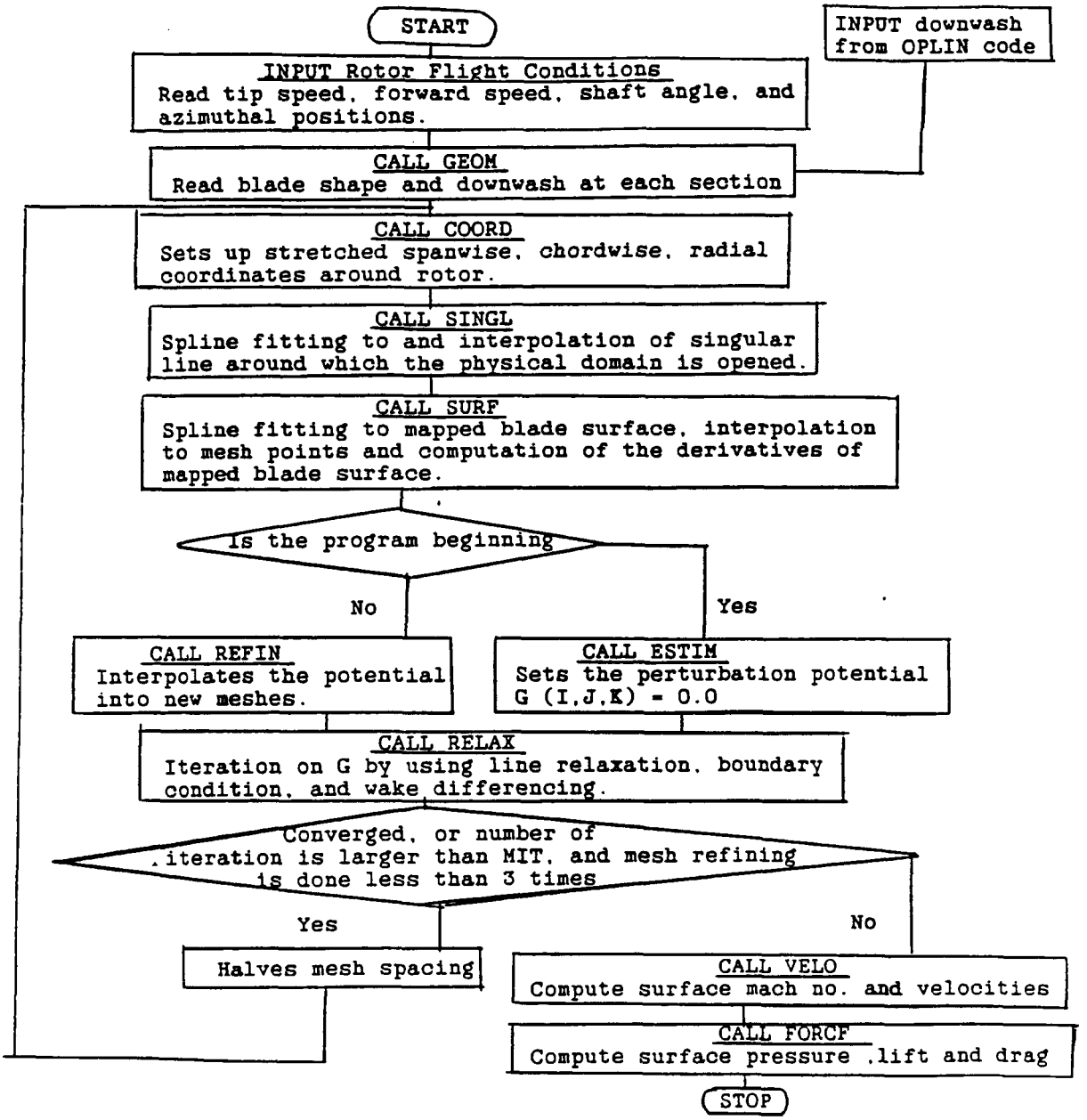

Figure 2.- Flow charts for the integration of programs TFAR1 and OPLIN.

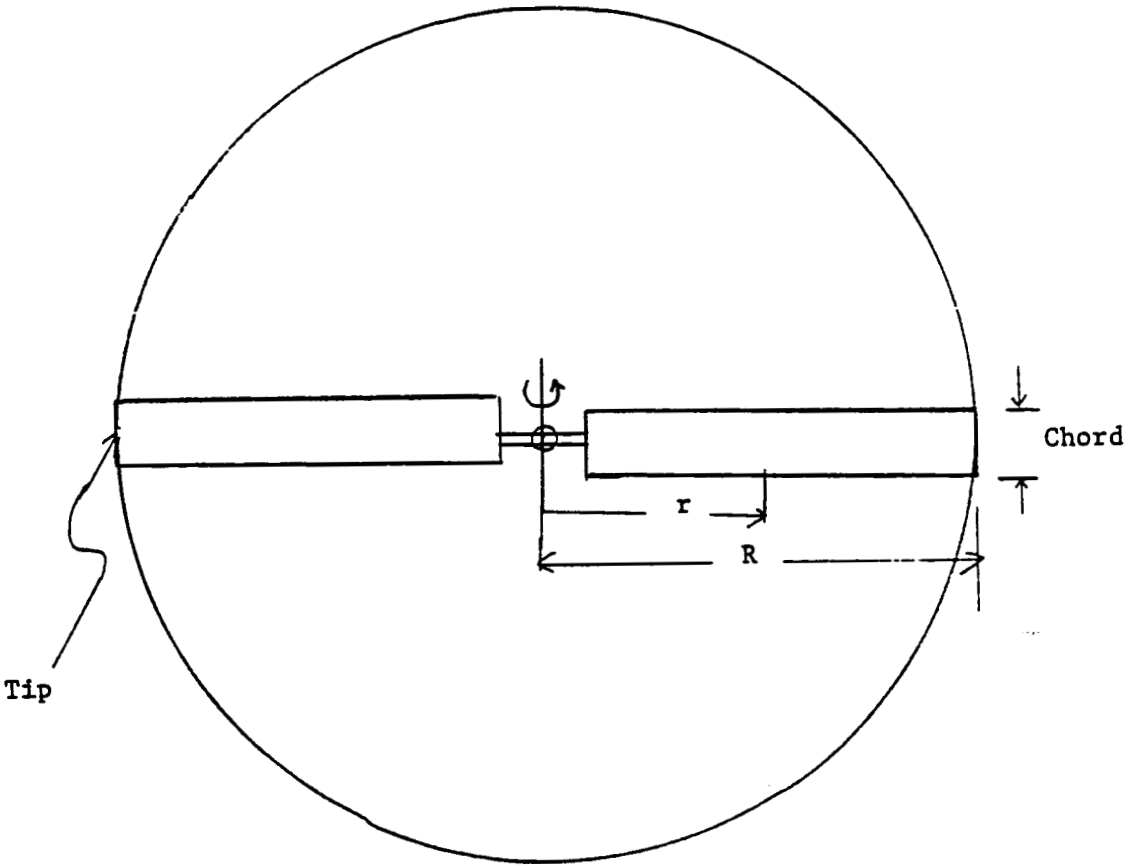

Figure 3.- Rotor blade geometry of pitch angle = 8°.

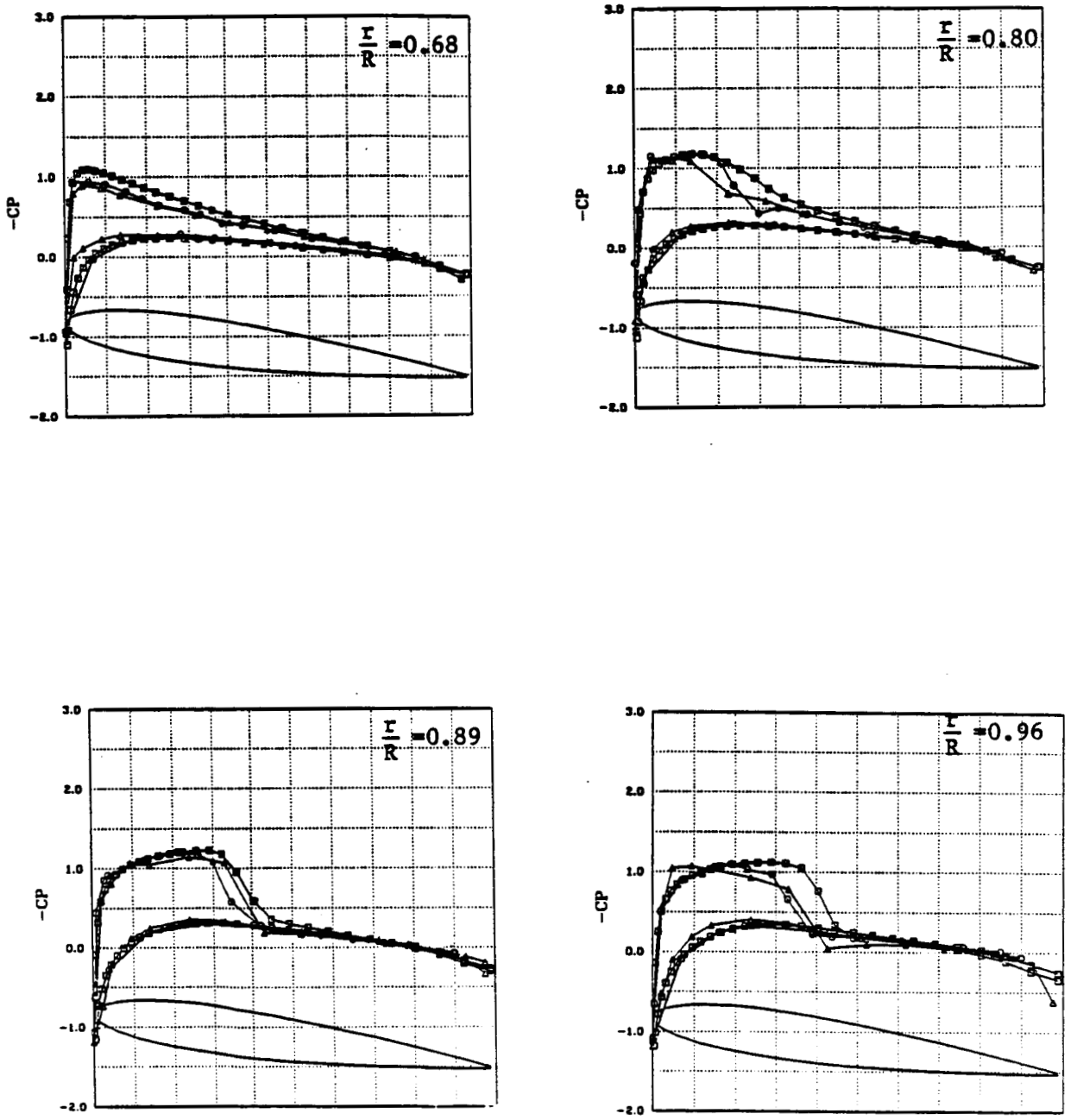

Figure 4.- Comparison of two calculated pressure distributions (Δ,□) with experiments (-○-) at tip Mach = 0.877 and pitch angle = 8°.

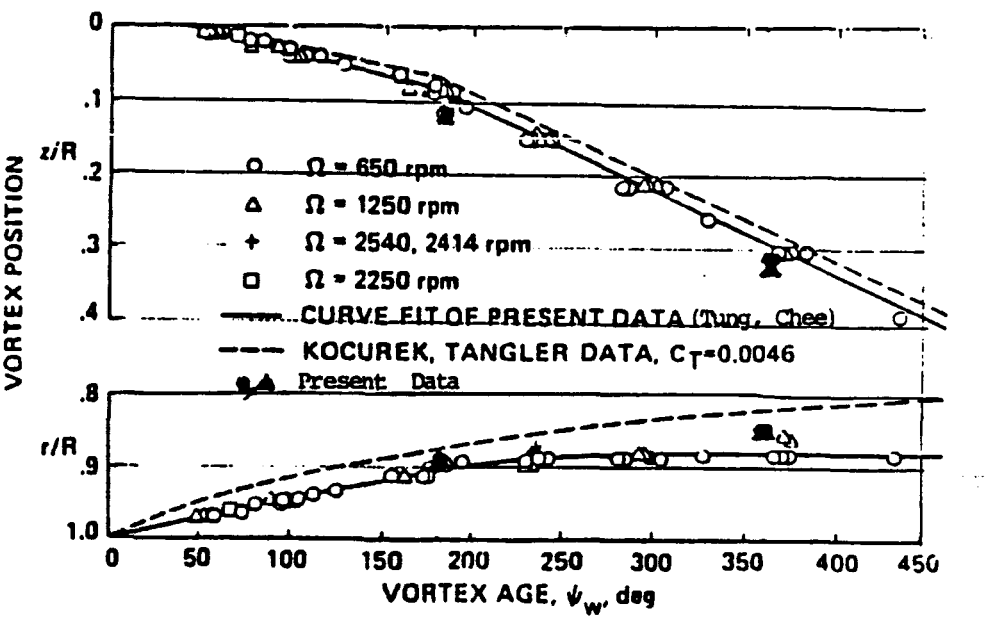

Figure 5.- Comparison of calculated tip vortex positions with experiments of reference 6.

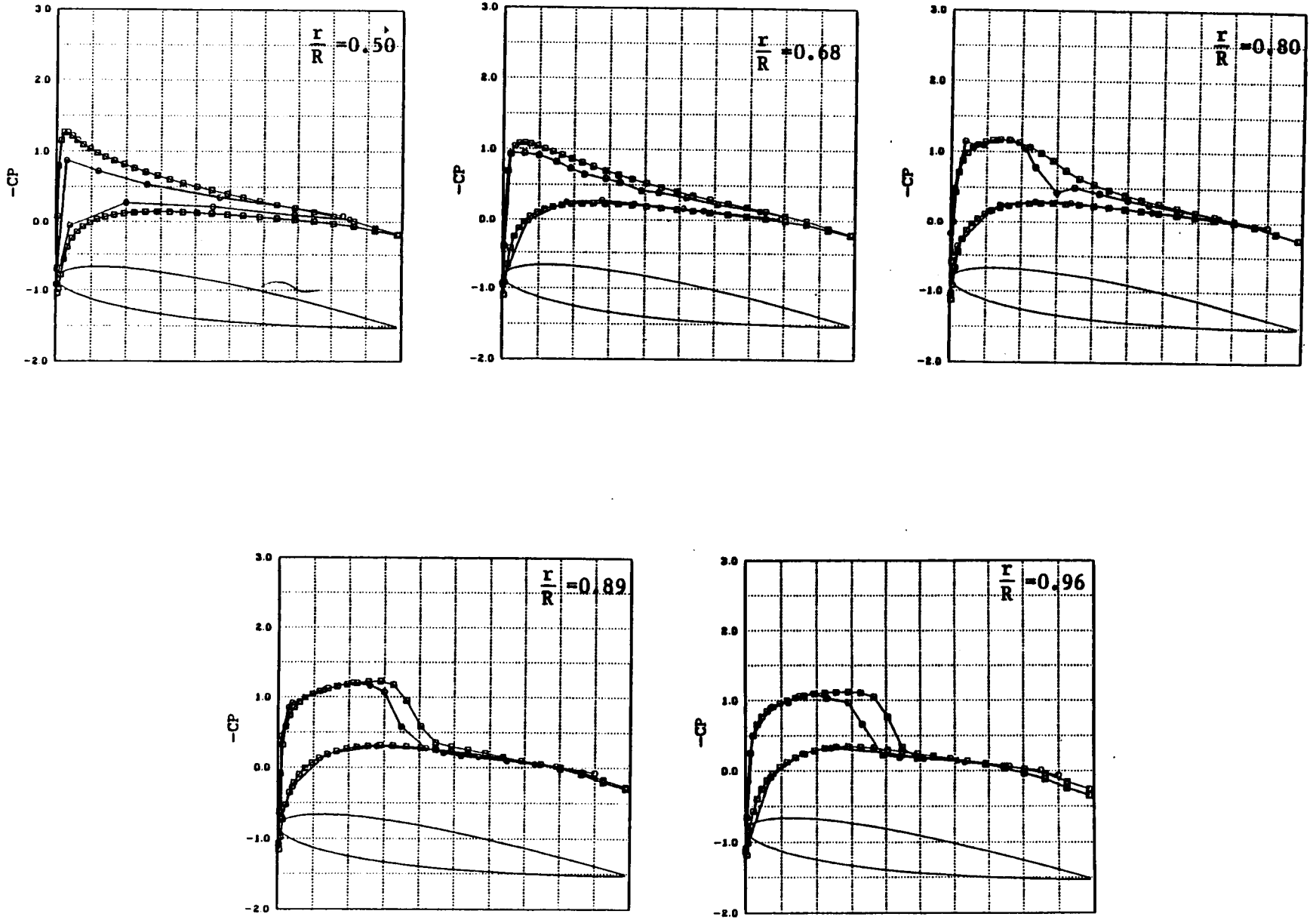

Figure 6.- Comparison of present calculated pressure distributions (⊡) with experiments (⊙) at tip Mach = 0.877 and pitch angle = 8°.

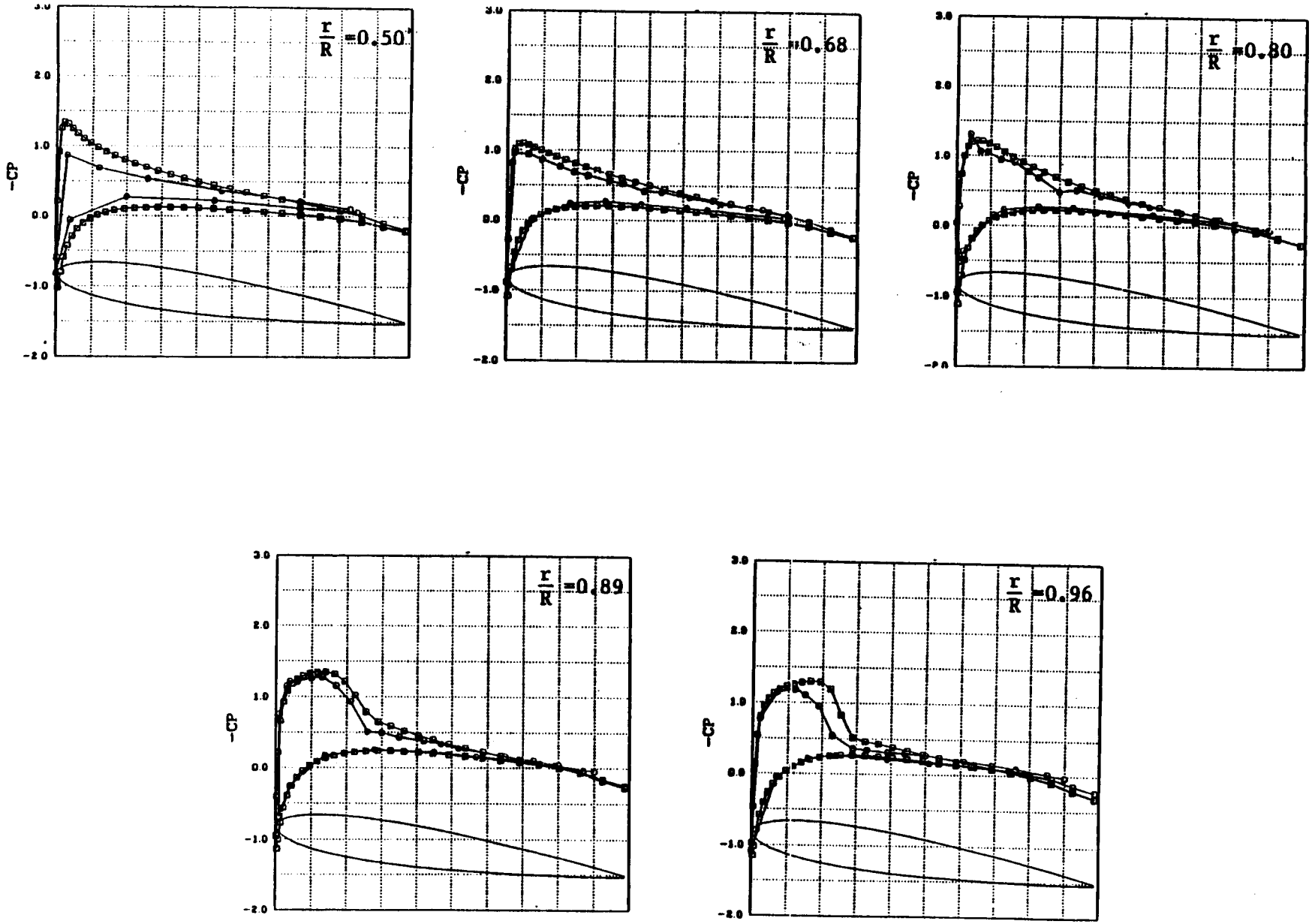

Figure 7.- Comparison of present calculated pressure distributions (-□-) with with experiments (-○-) at tip Mach = 0.794 and pitch angle = 8°.

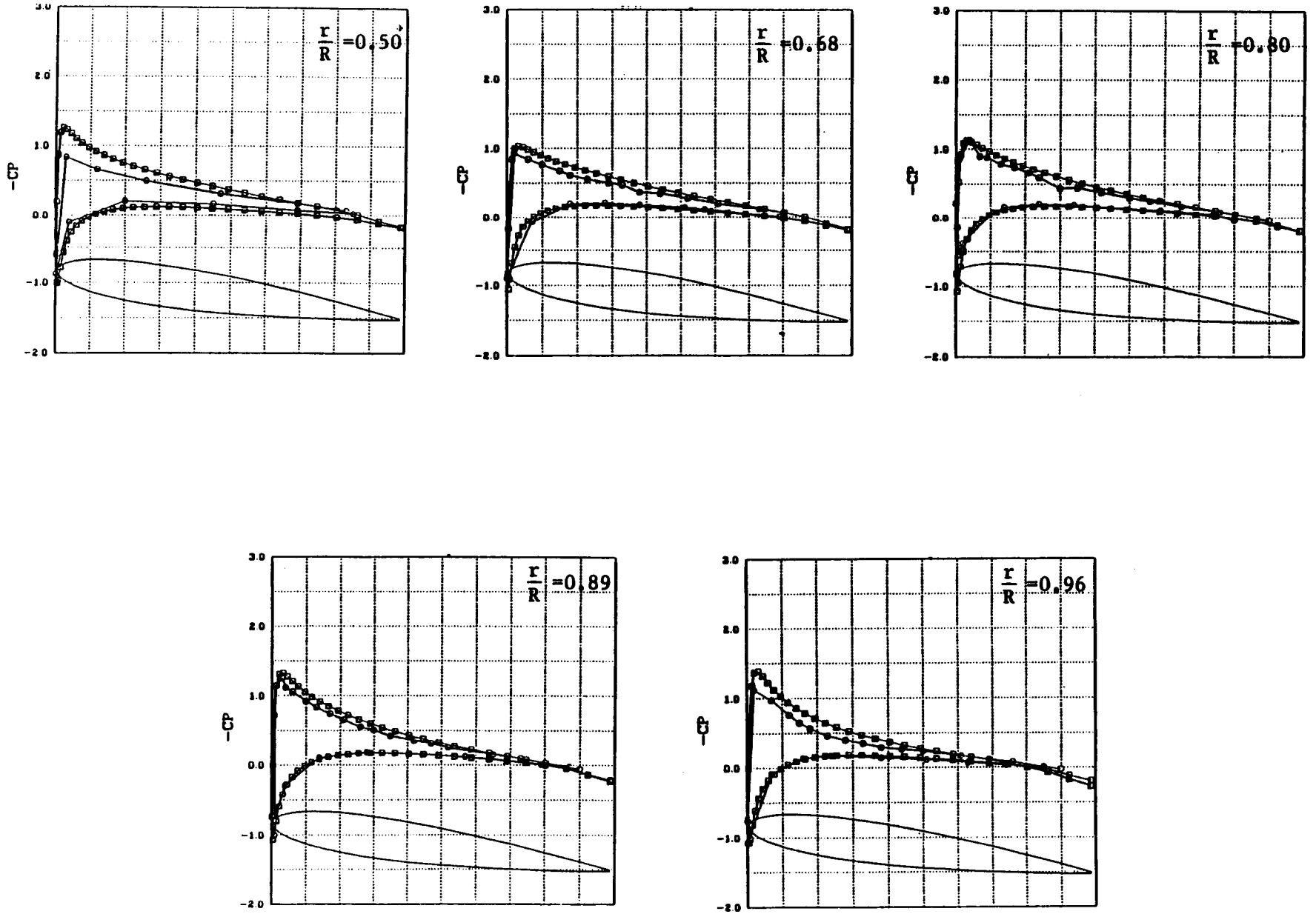

Figure 8.- Comparison of present calculated pressure distributions (⊡) with experiments (○) at tip Mach = 0.612 and pitch angle = 8°.

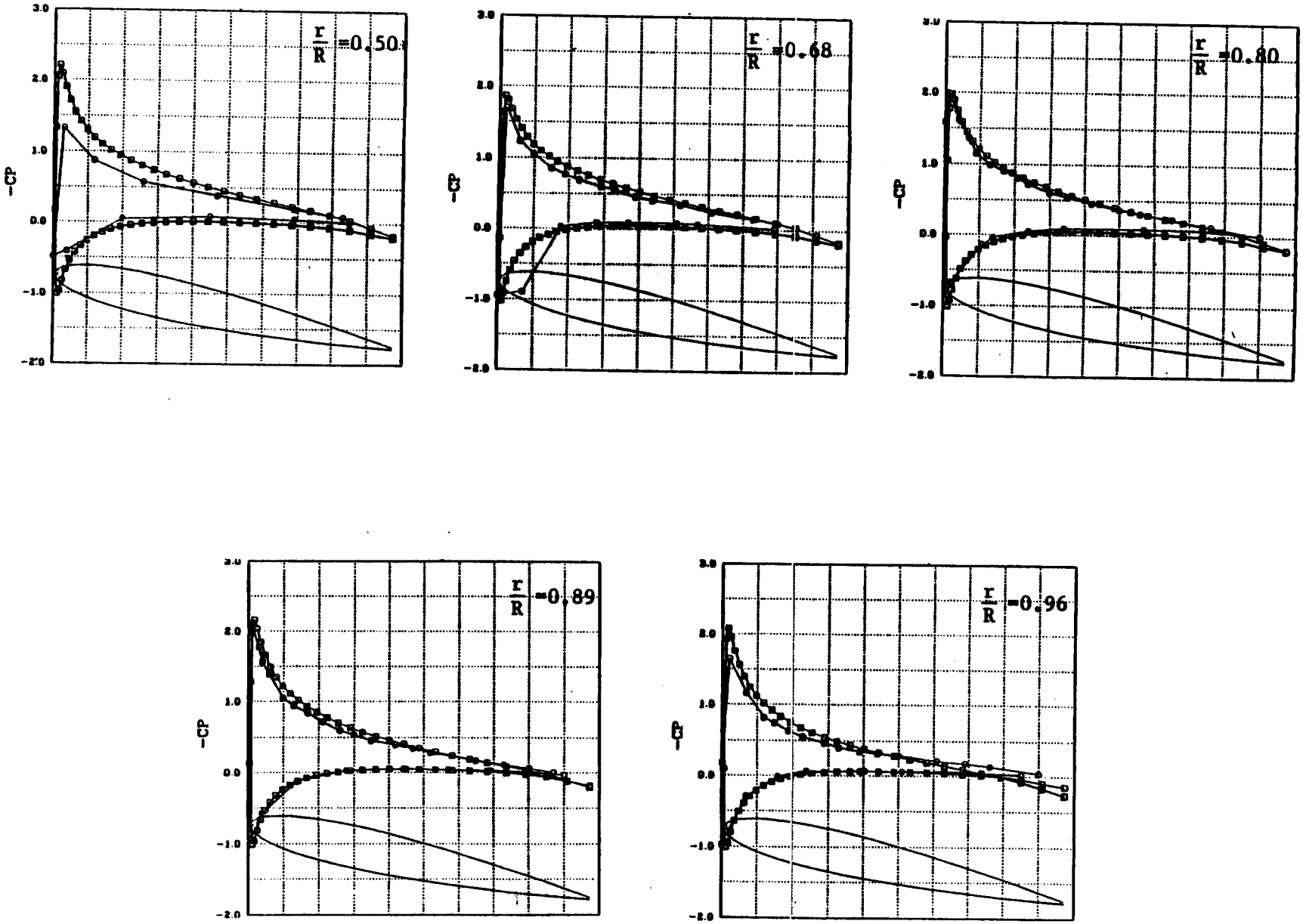

Figure 9.- Comparison of present calculated pressure distributions (⊡) with experiments (○) at tip Mach = 0.266 and pitch angle = 12°.

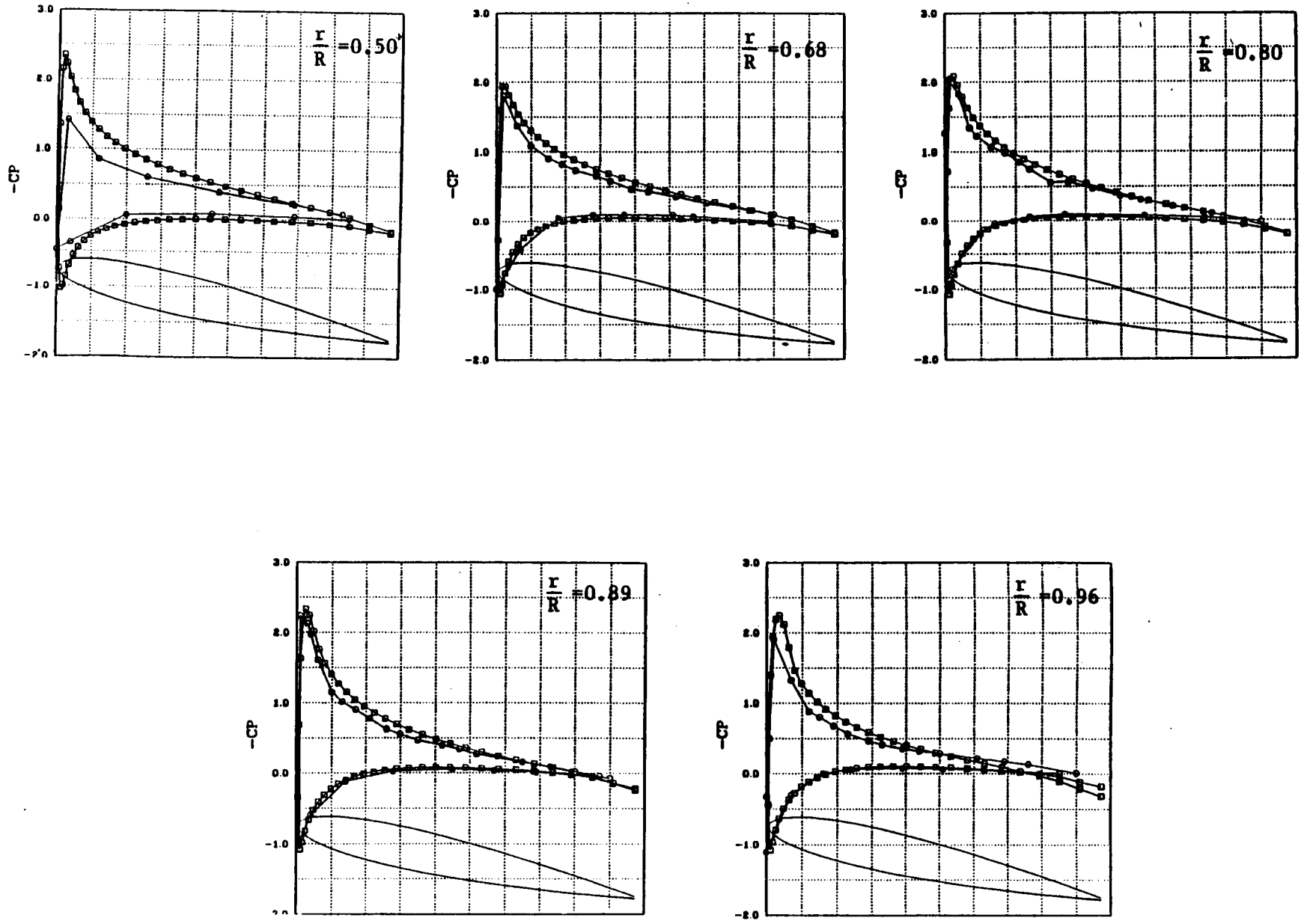

Figure 10.- Comparison of present calculated pressure distributions (⊏) with experiments (○) at tip Mach = 0.610 and pitch angle = 12°.

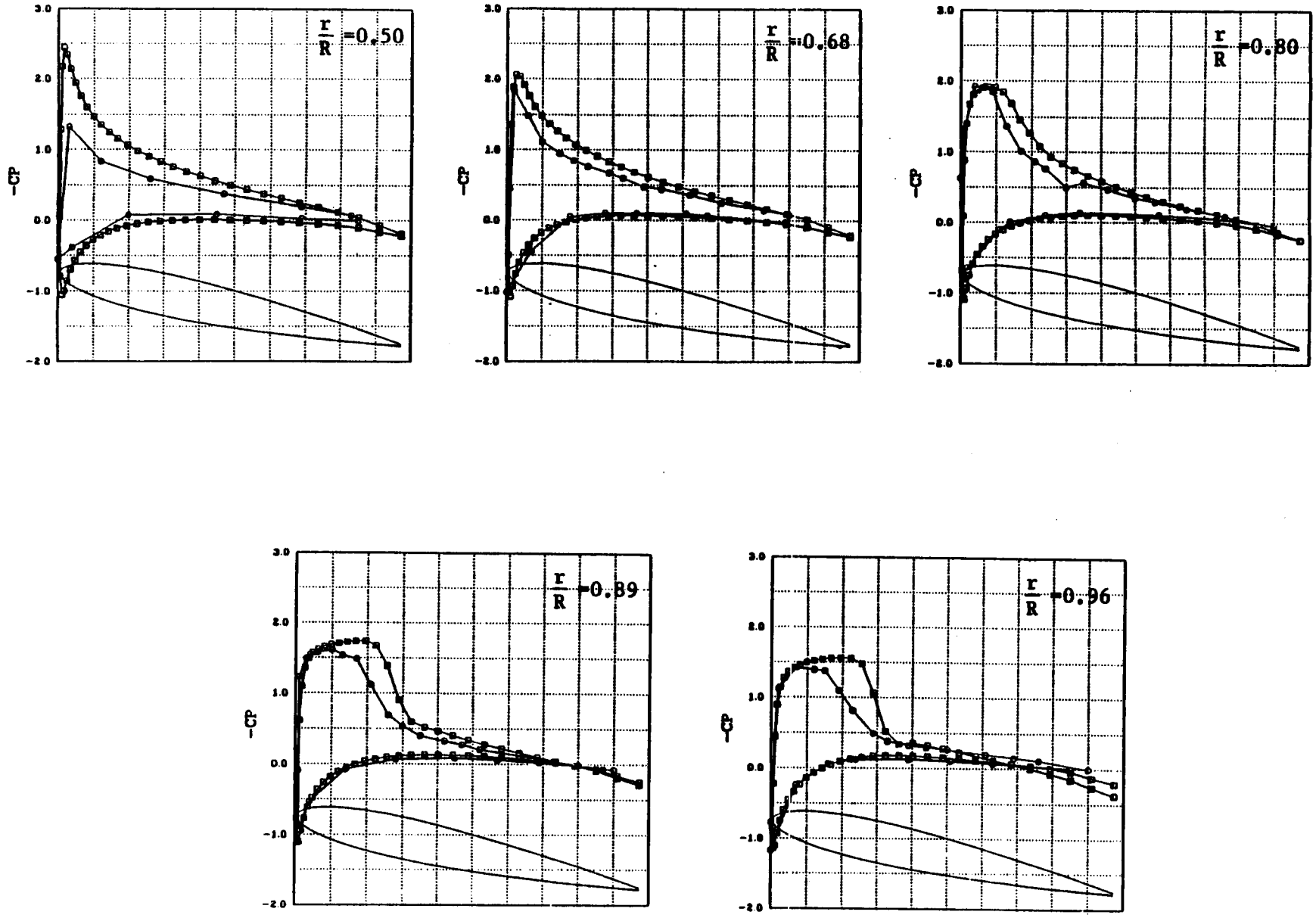

Figure 11.- Comparison of present calculated pressure distributions (⊡) with experiments (⊙) at tip Mach = 0.794 and pitch angle = 12°.

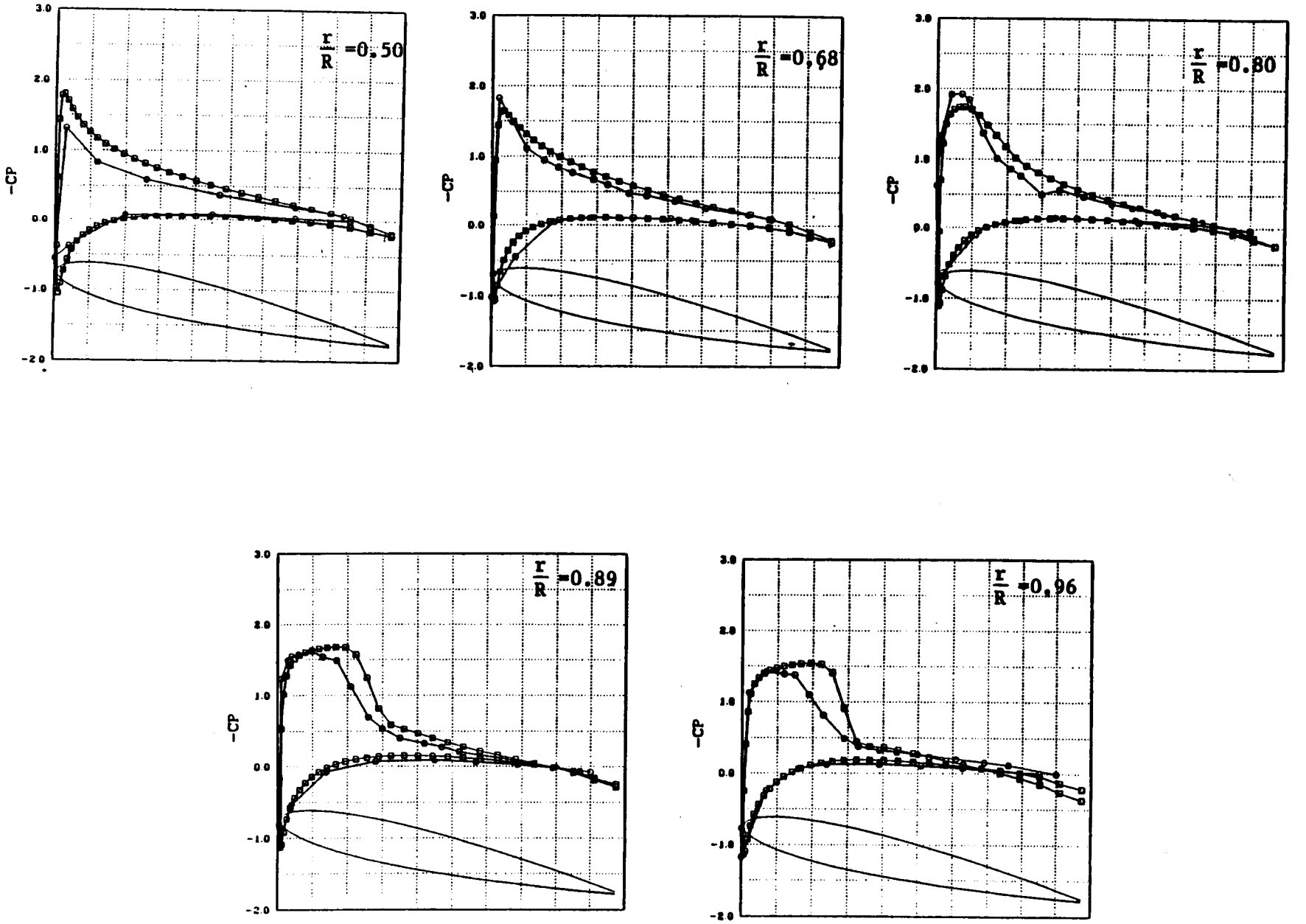

Figure 12.- Comparison of present calculated pressure distributions (⊡) with experiments (○) at tip Mach = 0.794 and pitch angle = 12° (with one vortex line correction.

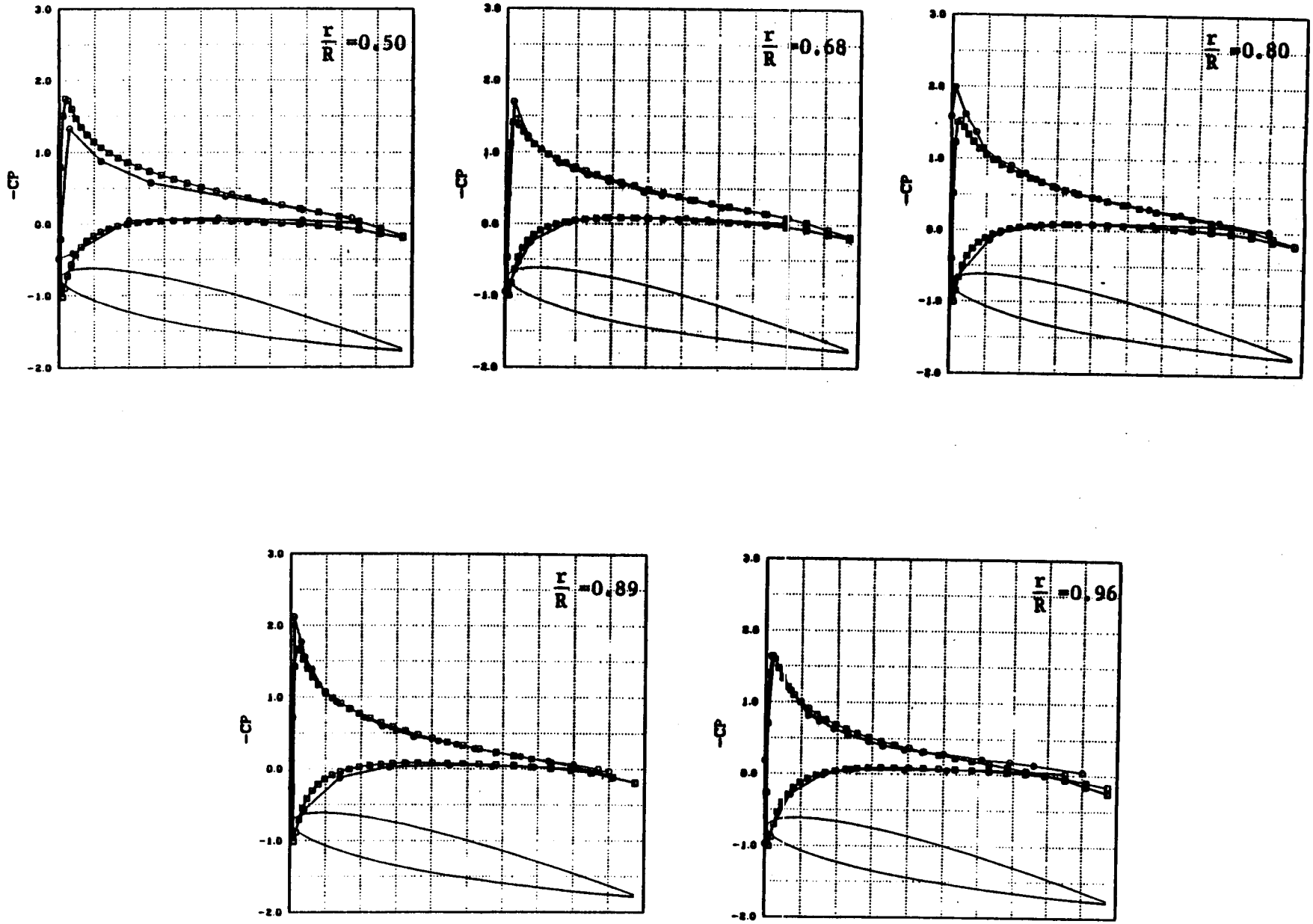

Figure 13.- Comparison of present calculated pressure distributions (⊡) with experiments (-o-) at tip Mach = 0.226 and pitch angle = 12° (with one vortex line correction).

NASA National Aeronautics and Space Administration

Report Documentation Page

1. Report No.	2. Government Accession No.	3. Recipient's Catalog No.
NASA TM-89494		

4. Title and Subtitle

Results of the Integration of a Transonic Full-Potential Analysis Program with a Free-Wake Lifting-Line Program for Hovering Rotors

5. Report Date
May 1987

6. Performing Organization Code

7. Author(s)

Song-Young Chung

8. Performing Organization Report No.
A-87193

10. Work Unit No.
505-61-51

9. Performing Organization Name and Address

Ames Research Center
Moffett Field, CA 94035

11. Contract or Grant No.

13. Type of Report and Period Covered
Technical Memorandum

12. Sponsoring Agency Name and Address

National Aeronautics and Space Administration
Washington, DC 20546

14. Sponsoring Agency Code

15. Supplementary Notes

Point of Contact: I-Chung Chang, Ames Research Center, M/S 260-1
Moffett Field, CA 94035 (415) 694-6396 or FTS 464-6396

16. Abstract

This report discusses the hovering performance predictions of the TFAR1 and OPLIN codes and the experimental data discussed in reference 6. The TFAR1 program solves the full-potential equation in a rotor-fixed coordinate system by use of the line relaxation method. The OPLIN program calculates the positions of wake vortices and rotor performance using the influence-coefficient-and-lifting-line method. The two programs are combined by adding the induced velocities from the OPLIN code to the near flow-field of the rotor from the TFAR1 code. Results of this investigation show that the TFAR1 program converges better with the downwash-coupling method than the twist correction method to include the wake downwash.

17. Key Words (Suggested by Author(s))	18. Distribution Statement
Rotor vortex interaction Transonic full-potential calculation	Unclassified-Unlimited Subject Category - 02

19. Security Classif. (of this report)	20. Security Classif. (of this page)	21. No. of pages	22. Price
Unclassified	Unclassified	23	A02

NASA FORM 1626 OCT 86